Article:
Song, H, Wignall, PB orcid.org/0000-0003-0074-9129, Song, H et al. (2 more authors) (2019) Seawater Temperature and Dissolved Oxygen over the Past 500 Million Years. Journal of Earth Science, 30 (2). pp. 236-243. ISSN 1674-487X

https://doi.org/10.1007/s12583-018-1002-2

doi: 10.1007/s12583-018-1002-2

Seawater temperature and dissolved oxygen over the past 500 million years

HaijunSong[1*], Paul B. Wignall[2], HuyueSong[1], Xu Dai[1], DaoliangChu[1]

[1]*State Key Laboratory of Biogeology and Environmental Geology, School of Earth Sciences, China University of Geosciences, Wuhan 430074, China*

[2]*School of Earth and Environment, University of Leeds, Leeds LS29JT, UK*

[*]Corresponding author: haijunsong@cug.edu.cn

ABSTRACT

Ocean temperature and dissolved oxygen concentrations are critical factors that control ocean productivity, carbon and nutrient cycles, and marine habitat. However,the evolution of these two factors in the geologic past are still unclear. Here, we use a new oxygen isotope database to establish the sea surfacetemperature(SST) curve in the past 500 million years. The database is composed of22,796 oxygen isotope values of phosphatic and calcareous fossils. The result shows two prolonged cooling events happened in the late Paleozoic and late Cenozoic, coinciding with two major ice ages indicated by continental glaciation data, and seven global warming eventsthat happened in the late Cambrian, Silurian-Devonian transition, late Devonian, Early Triassic, Toarcian, Late Cretaceous, and Paleocene-Eocene transition.The SSTs during these warming periods are about 5–30 °C higher than the present-day level.Oxygen contents of shallow seawater are calculated from temperature, salinity, and atmospheric oxygen. The results show that major dissolved oxygen valleys of surface seawater coincide with global warming events and ocean anoxic events. We propose that the combined effect of temperature and dissolved oxygen account for the long-term evolution of global oceanic redox state during the Phanerozoic.

Key Words: sea surfacetemperature, global warming, ocean anoxic event, dissolved

oxygen, Phanerozoic

0INTRODUCTION

Global warming is becoming a major environmental problem for humans in the twenty-first century. Global mean surface air temperature rose ~1°C in the past century and it likely that they will rise by>1°Ctowardthe end of thiscentury(Meinshausen et al., 2009, Brown and Caldeira, 2017). Rising ocean temperatures have profound impacts on reef ecosystems, triggering mass bleaching of corals(Hughes et al., 2017). Potentially severe consequences of global warming include thedeclines in dissolved oxygen (DO) in the ocean interior and an expansion in the area and volume of oceanic oxygen minimum zones(Stramma et al., 2008), which may further lead to significant changes in biogeochemical cycles and mass extinctions for marine organisms.

Ocean temperature and DO concentrations have varied greatly in the geologic time.For example, sea surface temperature(SST) warmed 4–8°C within a few thousand years at the Paleocene-Eocene transition about 55 million years (Myr) ago, which was accompanied by enhanced seawater anoxia and extinctions of benthic foraminifers(Kennett and Stott, 1991, Zachos et al., 2003, Dickson et al., 2012). The rapid warming of ~10°C at the Permian-Triassic transition about 252Myr ago is probably the most conspicuous example(Joachimski et al., 2012, Sun et al., 2012). The temperature rise and associated widespread oceanic anoxia are likely the main killing mechanism for the most severe extinction of marine organisms in the Phanerozoic Eon(Song et al., 2014, Penn et al., 2018).

The SST of ancient oceansis mainly assessed using oxygen isotope values fromfossil shells.A critical issue for oxygen isotope paleothermometry is the uncertainty of the composition of seawater $\delta^{18}O$ in deep time, whether it remained constant or changed significantly. Previous SST estimates in the Phanerozoic usually used an increased seawater $\delta^{18}O$ with ~1‰ per 10^8 years(Veizer et al., 2000, Veizer and Prokoph, 2015). In this scenario, the resulting SSTcurve cannot explain the two first-grade cooling events in the the early Paleozoic and middle Mesozoic because robust glacial evidence is

lacking(Royer et al., 2004). Additionally, the cold climates in the early Paleozoic conflict with extreme high level of atmospheric CO_2derived from the GEOCARBSULF model(Berner, 2006, Royer et al., 2014) and multiple proxies(Foster et al., 2017).Furthermore, recent clumped isotope evidence shows that the composition of seawater $\delta^{18}O$isalmost invariant over the past 500 Myr(Henkes et al., 2018). Here, we have assumed an invariant oxygen isotope composition of seawater to calculate temperatures in deep time.

Oxygen isotope measurements of carbonate fossils are useful in reconstructing ancient SSTs inthe younger Cenozoic and Mesozoic eras, but commonly yield questionable results for thePaleozoic Era(Grossman, 2012, Veizer and Prokoph, 2015). Paleozoic $\delta^{18}O$values from brachiopods show an extremely wide range in composition from ~0 ‰to –10 ‰ and,if the values are primary, thenthe calculated temperatures are unrealistically high, reaching 70 °C in the early Paleozoic(Grossman, 2012). One scenario is that the older the samples are,the more likely the$\delta^{18}O$values from these samples are diagenetically altered(Grossman et al., 1996).Recent studies have shown thatphosphate fossils (e.g.,conodont)are more reliable records of original seawater oxygen isotopes than biogenic carbonates(Joachimski et al., 2004, Trotter et al., 2008). Thousands of oxygen isotope measurements on Paleozoic andTriassic conodontshave been published in the past decades. These results, combined with numerous data from the Mesozoic and Cenozoic carbonate fossils, make it possible to establish a reliable SST curve for the past 500 Myr.

There is no means to directly measure seawater oxygen content of ancient oceans. The primary source of DO in surface seawater is air-sea exchange with atmospheric O_2, leading to approximate saturation. Therefore, the DO of surface seawater relies principally on atmospheric oxygen content, SST and salinity. A reliable O_2 curve for Phanerozoic atmosphere has been estimated by using the GEOCARBSULF model(Berner, 2006, Royer et al., 2014). In addition, the salinity changes of the oceans during the Phanerozoic have been constructed by a compiled dataset of volumes and masses of evaporate deposits(Hay et al., 2006). Thus, the evolution of seawater oxygen content in the geologic past can be assessedfrom estimated atmospheric O_2 and ocean salinity, and temperature that we constructed based on oxygen isotopes.

1 OXYGEN ISOTOPE DATASET

A total of 22,796 oxygen isotope measurements of carbonate/phosphate fossilsare selected to establish SST curve over the past 500 Myr (see Fig. 1 andDataset S1). The dataset is composed of published $\delta^{18}O$ measurements. A total of 8,782 $\delta^{18}O$ measurements are from the Phanerozoic database of Veizer and Prokoph(2015), 3,383 measurements are from Phanerozoic database of Grossman(2012), 1,677 measurements are from Cretaceous database of O'Brien et al.(2017), and 161 measurements are from Jurassic database of Dera et al.(2011). The other 8,793 $\delta^{18}O$ measurements have been compiled in this study. A total of 3,643$\delta^{18}O$ measurements are from phosphate fossils, including phosphatic brachiopods (46), conodonts (3,299), and fishes(298), while 19,153 $\delta^{18}O$ measurements are from carbonate fossils, including belemnites (1,663), bivalves (720), brachiopods (574), benthic foraminifers (129), planktonic foraminifers (15,500), gastropods (179), and coccoliths(388).

Not all data are used to reconstructing the SST curve. The selection of data depends mainly on the following three principles.First, only data from marine fossils that represent organisms living in the shallow water habitats are selected, i.e., shallow planktons (planktonic foraminifers), nektons (conodonts, fishes, and belemnites), and benthos (bivalves, brachiopods, and gastropods), but the bathyal benthic foraminifers are excluded. Second, only lower-paleolatitude data (between 40 °N and 40 °S) from well-preserved specimens are selected. Not only because $\delta^{18}O$ data from lower-paleolatitudes are abundant but also because of the strong temperature gradient between the equator and polarregions. For the regions between 40 °N and 40 °S, the latitude thermal gradient was much weaker under both present-day cool and Late Cretaceous warm climates (Sinninghe Damsté et al., 2010). Third, only$\delta^{18}O$datafrom phosphate fossils are selected for the Paleozoic Era because of the unreliability of $\delta^{18}O$ from carbonate fossils of this age. $\delta^{18}O$ from carbonate fossils have a great range in composition and the significant positive correlation with $\delta^{13}C$ (n = 4532, r = 0.64, p< 0.001, Fig. 2a), suggesting these data are probably affected by diagenetic alteration. However, there is no $\delta^{13}C$-$\delta^{18}O$ covariance for

the Mesozoic and Cenozoic carbonate fossils (n = 2066, r = 0.03, *p* = 0.171, Fig. 2b). Therefore, Mesozoic and Cenozoic $\delta^{18}O$ are compiled from both carbonate and phosphate fossils.

2METHODS

2.1 Paleo-sea surface temperature assessment from $\delta^{18}O$ dataset

Phosphate$\delta^{18}O$ values were converted to seawater temperatures by using the equation ofLécuyer et al.(2013), assuming an average $\delta^{18}O$ value of the ocean of –1‰:

$$t = 117.4 - 4.5 \times (\delta^{18}O_{PO4} - \delta^{18}O_{SW}) \times 1000$$

Where*t* is the sea surfacetemperature (°C), $\delta^{18}O_{PO4}$ is the O isotope composition of phosphate fossils (‰, VSMOW); $\delta^{18}O_{SW}$is the O isotope compositionof seawater(‰, VSMOW).

Seawater temperatures were calculated from the carbonate $\delta^{18}O$ by using equation of Hays and Grossman(1991):

$$t = 15.7 - 4.36 \times (\delta^{18}O_{Carb} - \delta^{18}O_{SW}) \times 1000 + 0.12 \times [(\delta^{18}O_{Carb} - \delta^{18}O_{SW}) \times 1000]^2$$

Where$\delta^{18}O_{Carb}$ is the O isotope composition of carbonate fossils (‰, VPDB).

2.2 Dissolved oxygen of shallow oceans

The solubility equation for oxygen is based on equation of Benson and Krause(1984):

$$DO = O_2[\frac{F(1 - P_{wv})(1 - \theta_o)}{k_{o,s}M_w}]$$

$$F = 1000 - 0.716582 \times S$$

$$P_{wv} = 10^{8.07131 - 1730.63/(233.426 + t)}/760$$

$$(1 - \theta_o) = 0.999025 + 1.426 \times 10^{-5}t - 6.436 \times 10^{-8}t^2$$

$$k_{o,s} = e^{3.71814 + 5596.17/T - 1049668/T^2 + S(0.0225034 - 13.6083/T + 2565.68/T^2)}$$

where *DO* is the standard air solubility concentrations of oxygen (mol/kg); O_2 is the atmospheric oxygen concentration; *F* is a salinity factor; *S* is the salinity of seawater (g/kg); P_{wv} is vapor pressure of water (atm); θ_o is a constant that depends on the second virial coefficient of oxygen; $k_{o,s}$ is Henry coefficient for oxygen (atm); M_w is mean molecular mass

of sea salt (18.0153 g/mol); *t* is temperature in degrees Celsius (°C); *T* = temperature in kelvins (K).

2.3 Dissolved oxygen of deep oceans

Deep ocean oxygen is calculated by using the equation of Sarmiento et al.(1988).

$$DO_d = DO_h - r(PO_{4d} - PO_{4h})$$

$$PO_{4h} = \frac{PO_{4d} f_{hd} - P_h}{f_{hd} + T}$$

Where DO_d is the dissolved oxygen of deep oceans; DO_h is the dissolved oxygen of high-latitude surface oceans; r is the Redfield ratio of oxygen consumption to phosphate production accompanying the oxidation of organic matter (r = ~169 for present ocean). PO_{4d} is the phosphate concentration of deep oceans; PO_{4h} is the phosphate concentration of high-latitude surface oceans; f_{hd} is a circulation parameter representing local convective overturning in deep water formation regions (f_{hd} = ~45 x $10^6 m^3\ s^{-1}$ for present ocean). P_h is the particulate rain of phosphate from the high-latitude deep water formation regions (P_h = 2.31 x 10^6mol C s^{-1} for present ocean). T is the large-scale thermohaline overturning (T = ~19 x $10^6 m^3\ s^{-1}$ for present ocean).

3 RESULTS

3.1 Estimatingseawater temperature

Oxygen isotope data from carbonate and phosphate fossils provide a late Cambrian to present SST curve (Fig. 3). These temperature estimates exhibit first-order variations characterized by warm climate in the Early Paleozoic-Devonian and Mesozoic-early Cenozoic, and cool climate in the late Paleozoic and late Cenozoic. The late Cambrian saw the warmest climate of the past 500 Myr with SSTreaching to ~45 °C. Although a rapid cooling occurred in the late Cambrian-Early Ordovician, the SSTof the Ordovician, Silurian, and Devonian is maintained at a high level around 30 °C. Another warm period occurred in the Mesozoic-early Cenozoic, during which the SSTfluctuated around 22 °C. Two cool intervalsare identified in the late Paleozoic and late Cenozoic, respectively. Seawater

temperature during these two cool intervals fluctuated around 17°C and has a lowest level of 12 °C in the late Carboniferous.

The second-order variations of temperatures derived from fossil oxygen isotopes reveal seven global warming events (GWEs): in the late Cambrian, Silurian-Devonian transition, Frasnian-Famennian transition, Early Triassic, Toarcian, Late Cretaceous, and Paleocene-Eocene transition(Fig. 3).The SSTsin the global warming intervals were significantly higher than present-day average temperatures, and witnessed a downward trend to younger intervals(Fig. 3). The SSTsduring the Paleocene-Eocene GWEand Mesozoic GWEs are about 5°Cand 10°Chigher than the present-day level, respectively. However, the SSTsin the late Cambrian and the early and lateDevonian look extraordinarily high, about 30°C and 15°C higher than the present level, respectively.

3.2 Estimatingdissolved oxygen of shallow seawater

Dissolved oxygen of oceans is influenced by many factorssuch as atmospheric oxygen level, temperature, organic productivity, and ocean currents(Sarmiento et al., 1988). However, for the surface seawater, it mainly depends on the former two because seawater oxygen dominantly comes from atmosphere by air-sea exchanging process. Marine primary producers generate and release a large amount of oxygen in the photic zones through photosynthesis. However, most of the oxygen escapes into the atmosphere within a short time because the surface seawater is near- saturated with oxygen. Therefore, the DO in the surface seawater depends primarily on factors that control the saturation of oxygen in seawaters such as temperature, atmospheric oxygen level, and salinity. The DO of surface seawater has a positive relationship with atmospheric oxygen level, but a negative relationship with temperature and salinity (Fig. 4a, b).

Surface seawateroxygen concentrations in the ancient near-tropic oceansare calculated based on the solubility equation for oxygen by using published salinity(Hay et al., 2006), atmospheric O_2(Royer et al., 2014), and the estimated temperature curve in this study (see Methods).The resultshowsfour major DO peaks in the late Ordovician-early Devonian (~250 μM), late Paleozoic (~350 μM), Middle-Late Triassic (~250 μM), and

Cretaceous-Cenozoic (~270 μM), and four major valleys in the late Cambrian-Early Ordovician (~110 μM), Late Devonian (~130 μM), Early Triassic (~170 μM), and Early Jurassic (~110 μM) (Fig. 5).

4DISCUSSION

4.1 The reliabilityof established temperature curve

There are still many uncertainties about reconstructing temperatures of ancient oceans. The critical issue is the composition of seawater oxygen isotope that we have discussed above. The second issue is the diverse habitats of different fossil groups. Although marine animals that were used to calculating temperature are shallow dwellers, most of them have a wide habitat in depth from 0 to 100-200 m. Therefore, the estimated temperature is is a mixture of valuesfrom shelf waters. The third issue is seawater pH. Changes in seawater pH normally result in oxygen isotope incorporation in carbonates and produce bias on $\delta^{18}O$-derived temperatures(Royer et al., 2004). However, oxygen isotopes from carbonate fossils are mainly from the post-Triassic interval when there was much less pCO_2 variation than in the Paleozoic(Royer et al., 2014, Foster et al., 2017). In addition, other factors such as icehouse climate and diagenesis could also potentially affect the accuracy of oxygen isotope paleothermometry(Grossman, 2012).For the temperature values calculated based on raw oxygen isotope data from different fossil groups, although some data deviate from the trend, the overall changeis consistent (Figs. 1, 3), suggesting the established SST curve is reliable.

4.2 The reliability of established dissolved oxygen curve

A critical limitation whenreconstructingtheoxygen content of surface seawater is theuncertain of paleo-O_2 and salinity. Atmospheric O_2 in geologic time is usually reconstructed through geochemical models, i.e., GEOCARB-style models (Bergman et al., 2004, Falkowski et al., 2005, Berner, 2006, Royer et al., 2014, Krause et al., 2018). However, these constructions are only moderately constrained by proxies. Charcoal is a

product of wildfire that occurs when oxygen content is over 15% (Belcher and McElwain, 2008). Sedimentary records show that charcoal is present in the sedimentary rocks of the past 400 Myr(Glasspool and Scott, 2010), suggesting oxygen content over 15% for much of the Phanerozoic. This observation is in keeping with geochemical models except in the Jurassic interval (Belcher and McElwain, 2008). Another limitation of reconstruction of seawater oxygen content is that paleo-salinity records are uncertain for the limited knowledge of the history of water on Earth. However, salinity of the past 500 Myr was likely within a narrow range of between 30‰ and 50‰(Hay et al., 2006).In this range, salinity only has a small contribution to the uncertainty of reconstruction of DO content (Fig. 4b).

4.3 The possible drivers of Phanerozoic temperature change

The first-order temperature variations are supported by robust and independent glaciological data for continental-scale ice sheets (Crowley and Berner, 2001) and carbonate clumped isotope data of fossil brachiopod and mollusk shells (Came et al., 2007, Henkes et al., 2018). For instance, the two major intervals of continental glaciationfrom the late Paleozoic (ca. 338–256 Myr ago) and late Cenozoic (ca. 40–0 Myr ago) (Crowell, 1999, Crowley and Berner, 2001)coincide closely with the two lowest-temperature intervals in the past 500 Myr(Figs. 1, 3). The transition from early Paleozoic warm climate to late Paleozoic cool climate can be also reflectedin the carbonate-clumped isotopes (Henkes et al., 2018). The estimated SST curve shows that the late Paleozoic ice age witnessed the coldest climate over the past 500 Myr. The lowest temperature of shallow seawater during the late Paleozoic is about 5 °C lower than the present-day level, which isin accord with the glaciological evidence that shows the longest and largest glacial period of the Phanerozoic at this time (Fielding et al., 2008).

Independent evidence is available for many of the second-order variations of temperatures. For example, the Paleocene-Eocene thermal maximum, PETM has been identified using multiple proxies in addition to oxygen isotope including foraminiferal magnesium/calcium ratios (Tripati and Elderfield, 2005) and TEX_{86} derived from the membrane lipids of marine picoplankton(Sluijs et al., 2006, Zachos et al., 2006).

ToarcianGWE is independently supported by the abrupt increase of atmospheric CO_2 obtained from fossil leaf stomatal frequency (McElwain et al., 2005). Early Triassic GWE reflected by marine conodont O isotopes coincided with the elevated air temperatures recorded by O isotopes from continental tetrapods(Rey et al., 2016).

Atmospheric CO_2 concentrations from the GEOCARBSULF model show a strong positive correlation between SST and CO_2 ($r = 0.853$, $N = 51$, $p << 0.001$,seeFig.6 and Table S2). Warm periods are characterized by higher CO_2 horizons, i.e., early Paleozoic, Mesozoic, and early Cenozoic. Cool periods are marked by lower CO_2 horizons such as late Paleozoic and late Cenozoic. However, the latest Ordovician ice age is an exception. Although temperature in this interval is the lowest of the Ordovician (Figs. 1, 3), CO_2 is at a high level of ~2500 ppm(Royer et al., 2014). It might be because the duration of the latest Ordovician glaciation was very short (~1 Myr)(Finnegan et al., 2011), but the GEOCARBSULF model generally has a time-step of 10 Myr(Royer et al., 2014). The overall striking correspondence between CO_2 concentrations and surface temperatures supports the proposal that high CO_2 concentrations drive or amplify high global temperatures(Berner, 1994, Crowley and Berner, 2001). In addition, temperature evolution calculated by oxygen isotope data seems to be associated with galactic cosmic ray flux(Shaviv and Veizer, 2003). In principle, the variations of cosmic ray flux likely contribute to the temperature evolution via controlling the formation of clouds at low latitudes(Shaviv and Veizer, 2003). Cold ages in the late Paleozoic and late Cenozoiccoincide with high cosmic ray fluxes, whereas most warm climate intervals are characterized by low cosmic ray fluxes, e.g., Cambrian, Devonian, Triassic, and Cretaceous. Only the mid-Jurassic warm period is an exception because it occurs during a time of low cosmic ray level(Shaviv and Veizer, 2003).

4.4 The drivers of Phanerozoic ocean redox state

The DO curve shows similar features of atmospheric O_2 derived from GEOCARBSULF model(Berner, 2006, Royer et al., 2014), suggesting atmospheric O_2 level is a major factor controlling long-term evolution of oxygen content of surface seawater. The second-order variations are associated intimately with temperature, e.g., valleys of DO closely coincide

with global warming events (see Fig. 5).

The reconstructed DO curve is supported by independent data on oceanic anoxic events (OAEs). Sedimentary and geochemical data show at least nine OAE intervals in the past 500 Myr, i.e., late Cambrian, Frasnian-Famennian transition, Early Triassic, Hettangian-Sinemurian, Toarcian, Aptian-Albian, Cenomanian-Turonian, Coniacian-Santonian, and Paleocene-Eocene transition (Meyer and Kump, 2008, Song et al., 2017, and Table S3). Most of those OAEscoincide with low levels of DO, especially the very low levels (< 150 μM) seen in the late Cambrian, late Devonian, and early Jurassic (Fig. 5). Additionally, OAEs show good correspondence with global warming events. Under a warm climate, surface seawaters absorb less oxygen, but probably also important is the likelihood of less efficient ocean circulation at these times(Sarmiento et al., 1988). Temperature is a major contributing factor on the rate of formation of deep water (f_{hd}) by controlling the strength of ocean thermohaline circulation. In modern oceans, $f_{hd}$is positively correlated with deep seawater oxygen(Fig. 4c). Therefore, deep ocean anoxia usually appeared under low f_{hd} associated with global warming events.

Oxygen content of surface seawater is a significant factor affecting the redox state of deep oceans. When surface DO is up to 1.5 times of present-level, it is difficult to cause deep-water anoxia even under low f_{hd}(Fig. 4c). Conversely, when surface DO fall to half, it can easily lead to anoxia indeep oceans. Another essential factor controlling the redox state of deep ocean is nutrient availability (represented by $PO_{4d} – PO_{4h}$)(Sarmiento et al., 1988), which has a negative relationship with deep seawater oxygen content (Fig. 4d). Some OAEs occurred in the periods of high surface DO levels, such as Cretaceous OAE1, 2, and 3, and Paleocene-Eocene OAE. High temperatures might be the most important factor for these OAEs by reducing the the solubility of oxygen and producing sluggish ocean circulations. In addition, global warming was usually accompanied by enhanced continental weathering and increased nutrient input to oceans(Jenkyns, 2010), which would further increase the rate of oxygen consumption and lead to a global OAE faster.

ACKNOWLEDGEMENTS

We thank Z. Qiu for collecting data, J. Veizer for comments on earlier drafts, and D.L. Royer for providing atmospheric oxygen and carbon dioxide data.This study is supported by the National Natural Science Foundation of China (41821001, 41622207, 41530104, 41661134047), the State Key R&D project of China (2016YFA0601100), and the Strategic Priority Research Program of Chinese Academy of Sciences (XDB26000000), a Marie Curie Fellowship (H2020-MSCA-IF-2015-701652), and the Natural Environment Research Council's Eco-PT project (NE/P01377224/1), which is a part of the Biosphere Evolution, Transitions and Resilience Program (BETR).

References

Belcher, C. M. ,McElwain, J. C., 2008. Limits for combustion in low O_2 redefine paleoatmospheric predictions for the mesozoic. *Science*, 321(5893): 1197–1200. doi: 10.1126/science.1160978

Benson, B. B. ,Krause, D., 1984. The concentration and isotopic fractionation of oxygen dissolved in freshwater and seawater in equilibrium with the atmosphere. *Limnology and Oceanography*, 29(3): 620–632. doi: 10.4319/lo.1984.29.3.0620

Bergman, N. M., Lenton, T. M. ,Watson, A. J., 2004. COPSE: A new model of biogeochemical cycling over Phanerozoic time. *American Journal of Science*, 304(5): 397–437. doi: 10.2475/ajs.304.5.397

Berner, R. A., 1994. GEOCARB II: A revised model of atmospheric CO_2 over Phanerozoic time. *American Journal of Science*, 294: 56–91. doi: 10.2475/ajs.301.2.182

Berner, R. A., 2006. GEOCARBSULF: A combined model for Phanerozoic atmospheric O_2 and CO_2. *Geochimica et Cosmochimica Acta*, 70(23): 5653–5664. doi: 10.1016/j.gca.2005.11.032

Brown, P. T. ,Caldeira, K., 2017. Greater future global warming inferred from Earth's recent energy budget. *Nature*, 552: 45–50. doi: 10.1038/nature24672

Came, R. E., Eiler, J. M., Veizer, J., et al., 2007. Coupling of surface temperatures and atmospheric CO_2 concentrations during the Palaeozoic era. *Nature*, 449: 198–201. doi: 10.1038/nature06085

Crowell, J. C., 1999. Pre-Mesozoic Ice Ages: Their Bearing on Understanding the Climate System. Geological Society of America. 112

Crowley, J. K. ,Berner, R. A., 2001. CO_2 and climate change. *Science*, 292: 870–872. doi: 10.1126/science.1061664

Dera, G., Brigaud, B., Monna, F., et al., 2011. Climatic ups and downs in a disturbed Jurassic world. *Geology*, 39(3): 215–218. doi: 10.1130/g31579.1

Dickson, A. J., Cohen, A. S. ,Coe, A. L., 2012. Seawater oxygenation during the Paleocene-Eocene Thermal Maximum. *Geology*, 40(7): 639–642. doi: 10.1130/g32977.1

Falkowski, P. G., Katz, M. E., Milligan, A. J., et al., 2005. The rise of oxygen over the past 205 million years and the evolution of large placental mammals. *Science*, 309(5744): 2202–2204. doi: 10.1126/science.1116047

Fielding, C. R., Frank, T. D. ,Isbell, J. L., 2008. The late Paleozoic ice age-A review of current understanding and synthesis of global climate patterns. In: Fielding, C. R., Frank, T. D. ,Isbell, J. L., eds. Resolving the Late Paleozoic Ice Age In Time And Space, 441. 343–354

Finnegan, S., Bergmann, K., Eiler, J. M., et al., 2011. The magnitude and duration of Late Ordovician–Early Silurian glaciation. *Science*, 331(6019): 903–906. doi: 10.1126/science.1200803

Foster, G. L., Royer, D. L. ,Lunt, D. J., 2017. Future climate forcing potentially without precedent in the last 420 million years. *Nature Communications*, 8: 14845. doi: 10.1038/ncomms14845

Glasspool, I. J. ,Scott, A. C., 2010. Phanerozoic concentrations of atmospheric oxygen reconstructed from sedimentary charcoal. *Nature Geoscience*, 3(9): 627–630. doi: 10.1038/ngeo923

Grossman, E. L., Mii, H. S., Zhang, C. L., et al., 1996. Chemical variation in Pennsylvanian brachiopod shells; diagenetic, taxonomic, microstructural, and seasonal effects. *Journal of Sedimentary Research*, 66(5): 1011–1022. doi: 10.1306/D4268469-2B26-11D7-8648000102C1865D

Grossman, E. L., 2012. Oxygen isotope stratigraphy. In: Gradstein, F. M., Ogg, J. G., Schmitz, M. D., et al., eds. The Geologic Time Scale 2012, Elsevier. 195–220

Hay, W. W., Migdisov, A., Balukhovsky, A. N., et al., 2006. Evaporites and the salinity of the ocean during the Phanerozoic: Implications for climate, ocean circulation and life. *Palaeogeography, Palaeoclimatology, Palaeoecology*, 240(1-2): 3–46. doi: 10.1016/j.palaeo.2006.03.044

Hays, P. D. ,Grossman, E. L., 1991. Oxygen isotopes in meteoric calcite cements as indicators of continental paleoclimate. *Geology*, 19(5): 441–444. doi: 10.1130/0091-7613(1991)019<0441:OIIMCC>2.3.CO;2

Henkes, G. A., Passey, B. H., Grossman, E. L., et al., 2018. Temperature evolution and the oxygen isotope composition of Phanerozoic oceans from carbonate clumped isotope thermometry. *Earth and Planetary Science Letters*, 490: 40–50. doi: 10.1016/j.epsl.2018.02.001

Hughes, T. P., Kerry, J. T., Álvarez-Noriega, M., et al., 2017. Global warming and recurrent mass bleaching of corals. *Nature*, 543: 373–377. doi: 10.1038/nature21707

Jenkyns, H. C., 2010. Geochemistry of oceanic anoxic events. *Geochemistry, Geophysics, Geosystems*, 11(3): Q03004. doi: 10.1029/2009GC002788

Joachimski, M. M., van Geldern, R., Breisig, S., et al., 2004. Oxygen isotope evolution of biogenic calcite and apatite during the Middle and Late Devonian. *International Journal of Earth Sciences*, 93(4): 542–553. doi: 10.1007/s00531-004-0405-8

Joachimski, M. M., Lai, X., Shen, S., et al., 2012. Climate warming in the latest Permian and the Permian–Triassic mass extinction. *Geology*, 40(3): 195–198. doi: 10.1130/g32707.1

Kennett, J. P. ,Stott, L. D., 1991. Abrupt deep-sea warming, palaeoceanographic changes and benthic extinctions at the end of the Paleocene. *Nature*, 353(6341): 225–229. doi: 10.1038/353225a0

Krause, A. J., Mills, B. J. W., Zhang, S., et al., 2018. Stepwise oxygenation of the Paleozoic atmosphere. *Nature Communications*, 9(1): 4081. doi: 10.1038/s41467-018-06383-y

Lécuyer, C., Amiot, R., Touzeau, A., et al., 2013. Calibration of the phosphate $\delta^{18}O$ thermometer with carbonate–water oxygen isotope fractionation equations. *Chemical Geology*, 347: 217–226. doi: 10.1016/j.chemgeo.2013.03.008

McElwain, J. C., Wade-Murphy, J. ,Hesselbo, S. P., 2005. Changes in carbon dioxide during an oceanic anoxic event linked to intrusion into Gondwana coals. *Nature*, 435: 479–482. doi: 10.1038/nature03618

Meinshausen, M., Meinshausen, N., Hare, W., et al., 2009. Greenhouse-gas emission targets for limiting global warming to 2 °C. *Nature*, 458: 1158–1162. doi: 10.1038/nature08017

Meyer, K. M. ,Kump, L. R., 2008. Oceanic euxinia in Earth history: causes and consequences. *Annual Review of Earth and Planetary Sciences*, 36: 251–288. doi: 10.1146/annurev.earth.36.031207.124256

O'Brien, C. L., Robinson, S. A., Pancost, R. D., et al., 2017. Cretaceous sea-surface temperature evolution: Constraints from TEX_{86} and planktonic foraminiferal oxygen isotopes. *Earth-Science Reviews*, 172: 224–247. doi: 10.1016/j.earscirev.2017.07.012

Penn, J. L., Deutsch, C., Payne, J. L., et al., 2018. Temperature-dependent hypoxia explains biogeography and severity of end-Permian marine mass extinction. *Science*, 362(6419): eaat1327. doi: 10.1126/science.aat1327

Rey, K., Amiot, R., Fourel, F., et al., 2016. Global climate perturbations during the Permo-Triassic mass extinctions recorded by continental tetrapods from South Africa. *Gondwana Research*, 37: 384–396. doi: 10.1016/j.gr.2015.09.008

Royer, D. L., Berner, R. A., Montanez, I. P., et al., 2004. CO_2 as a primary driver of Phanerozoic climate. *GSA Today*, 14(3): 4–10. doi: 10.1130/1052-5173(2004)014<0004:CAAPDO>2.0.CO:2

Royer, D. L., Donnadieu, Y., Park, J., et al., 2014. Error analysis of CO_2 and O_2 estimates from the long-term geochemical model GEOCARBSULF. *American Journal of Science*, 314(9): 1259–1283. doi: 10.2475/09.2014.01

Sarmiento, J. L., Herbert, T. D. ,Toggweiler, J. R., 1988. Causes of anoixia in the world ocean. *Global Biogeochemical Cycles*, 2(2): 115–128. doi: 10.1029/GB002i002p00115

Shaviv, N. J. ,Veizer, J., 2003. Celestial driver of Phanerozoic climate? *GSA Today*, 13: 4–10. doi: 10.1130/1052-5173(2003)013<0004:CDOPC>2.0.CO;2

Sinninghe Damsté, J. S., van Bentum, E. C., Reichart, G.-J., et al., 2010. A CO_2 decrease-driven cooling and increased latitudinal temperature gradient during the mid-Cretaceous Oceanic Anoxic Event 2. *Earth and Planetary Science Letters*, 293(1): 97–103. doi: 10.1016/j.epsl.2010.02.027

Sluijs, A., Schouten, S., Pagani, M., et al., 2006. Subtropical Arctic Ocean temperatures during the Palaeocene/Eocene thermal maximum. *Nature*, 441: 610–613. doi: 10.1038/nature04668

Song, H., Wignall, P. B., Chu, D., et al., 2014. Anoxia/high temperature double whammy during the Permian-Triassic marine crisis and its aftermath. *Scientific Reports*, 4: 4132. doi: 10.1038/srep04132

Song, H., Jiang, G., Poulton, S. W., et al., 2017. The onset of widespread marine red beds and the evolution of ferruginous oceans. *Nature Communications*, 8: 399. doi: 10.1038/s41467-017-00502-x

Stramma, L., Johnson, G. C., Sprintall, J., et al., 2008. Expanding oxygen-minimum zones in the tropical oceans. *Science*, 320(5876): 655–658. doi: 10.1126/science.1153847

Sun, Y., Joachimski, M. M., Wignall, P. B., et al., 2012. Lethally hot temperatures during the Early Triassic greenhouse. *Science*, 338(6105): 366–370. doi: 10.1126/science.1224126

Tripati, A. ,Elderfield, H., 2005. Deep-sea temperature and circulation changes at the Paleocene-Eocene thermal maximum. *Science*, 308(5730): 1894–1898. doi: 10.1126/science.1109202

Trotter, J. A., Williams, I. S., Barnes, C. R., et al., 2008. Did cooling oceans trigger Ordovician biodiversification? Evidence from conodont thermometry. *Science*, 321(321): 550–554. doi: 10.1126/science.1155814

Veizer, J., Godderis, Y. ,François, L. M., 2000. Evidence for decoupling of atmospheric CO_2 and global climate during the Phanerozoic eon. *Nature*, 408(6813): 698–701. doi: 10.1038/35047044

Veizer, J. ,Prokoph, A., 2015. Temperatures and oxygen isotopic composition of Phanerozoic oceans. *Earth-Science Reviews*, 146: 92–104. doi: 10.1016/j.earscirev.2015.03.008

Zachos, J. C., Wara, M. W., Bohaty, S., et al., 2003. A transient rise in tropical sea surface temperature during the Paleocene-Eocene thermal maximum. *Science*, 302(5650): 1551–1554. doi: 10.1126/science.1090110

Zachos, J. C., Schouten, S., Bohaty, S., et al., 2006. Extreme warming of mid-latitude coastal ocean during the Paleocene-Eocene Thermal Maximum: Inferences from TEX_{86} and isotope data. *Geology*, 34(9): 737–740. doi: 10.1130/g22522.1

Figure Captions

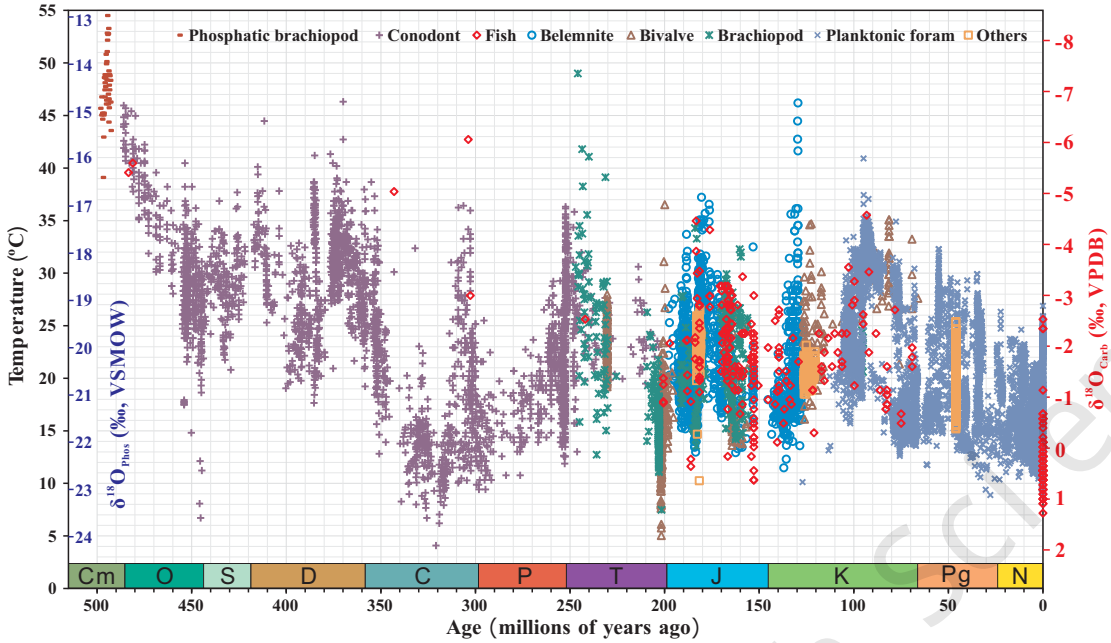

Figure1. Raw oxygen isotope data used for reconstructing sea surfacetemperatures over the past 500 million years. A total of 22,796 oxygen isotopic measurements are used(see Dataset S1). The scale of $\delta^{18}O_{Phos}$is used for phosphatic fossils including phosphatic brachiopod, conodont, and fish. The scale of $\delta^{18}O_{Carb}$is used for carbonate fossils including belemnite, bivalve, brachiopod, planktonic foraminifer, and others. The scale of temperature is used for all fossils. Dark red short line: phosphatic brachiopod; purple plus sign: conodont; red diamond: fish; blue circle: belemnite; Dark red triangle: bivalve; green star: brachiopod; blue multiple sign: planktonic foraminifer; orange square: other carbonate fossils.

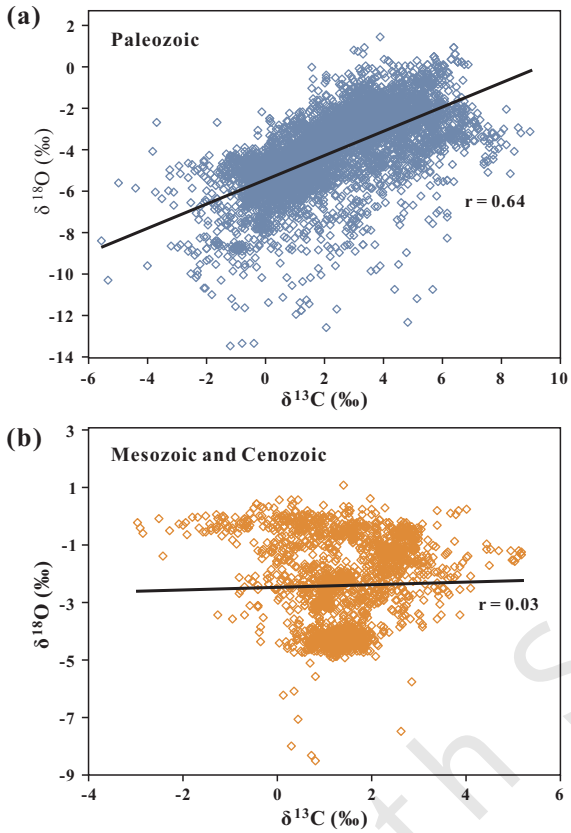

Figure 2. Cross plots of carbon and oxygen isotopes of carbonate fossils from Phanerozoic.(a) Cross plot of Paleozoic $\delta^{13}C$ versus $\delta^{18}O$ showing a clear positive relationship (n = 4532, r = 0.64, p< 0.001). **(b)** Mesozoic and Cenozoic $\delta^{13}C$ versus $\delta^{18}O$. There is no $\delta^{13}C$-$\delta^{18}O$ covariance for the entire data (n = 2066, r = 0.03, p = 0.171). Data are from ref. (Grossman, 2012).

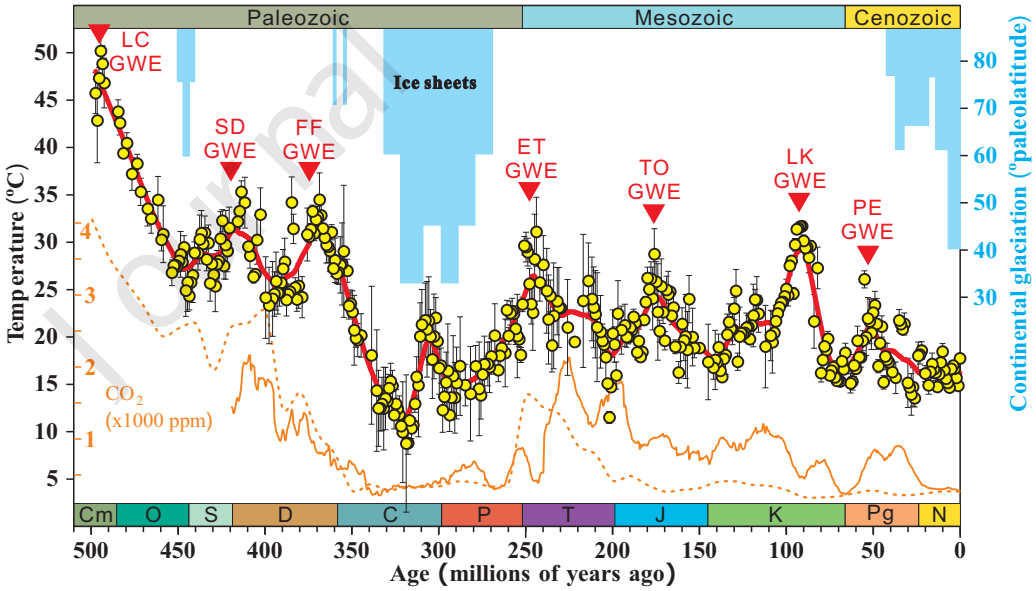

Figure3. Low-latitude sea surfacetemperatures, continental-scale ice sheets, and CO_2 concentrations for the past 500 million years. Each temperature dot presents the mean value per one million years (data see Table S1). Vertical error bars show 95% confidence intervals. The smoothed curve is locally weighted linear regressions (LOWESS, red line). Glaciological data for ice sheets are modified from (Crowley and Berner, 2001). Atmospheric CO_2 concentrations are from the GEOCARBSULF model (orange dash line)(Royer et al., 2014)and multiple proxies (orange solid line)(Foster et al., 2017). Global warming events (GWEs) are peaks identified from the temperature curve. The peak the late Carboniferousis not considered as a GWE because the maximum temperature during this interval is only ~20 °C, which is lower than most of Phanerozoic temperatures. LC, late Cambrian; SD, Silurian-Devonian; FF, Frasnian-Famennian; ET, Early Triassic; TO, Toarcian; LK, Late Cretaceous; PE, Paleocene-Eocene.

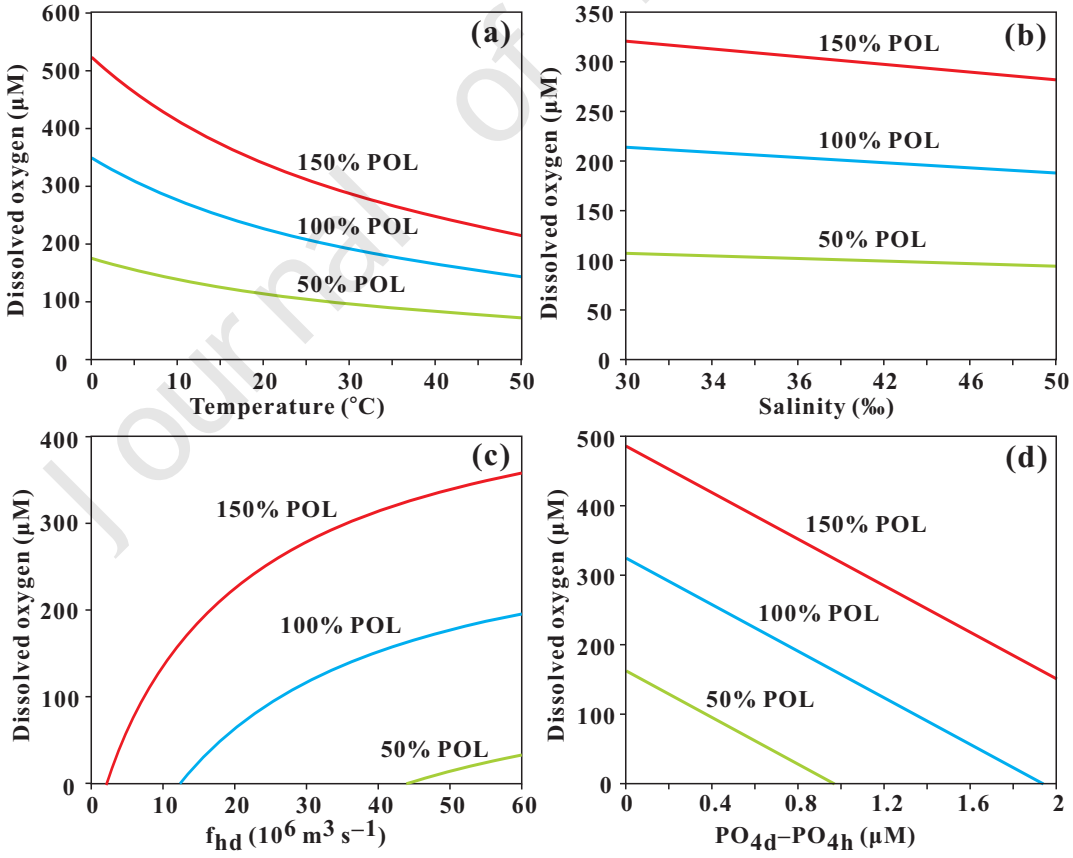

Figure 4.The relationship between seawater oxygen concentration and impact factors in the oceans. (a) Surface seawater oxygen concentration versus temperature (at salinity = 35‰). **(b)**Surface seawater oxygen concentration versus salinity (at temperature = 25 °C). **(c)** Deep-water oxygen concentration versus rate of deep-water formation (represented by f_{hd}). **(d)** Deep-water oxygen concentration versus phosphorus availability (represented by $PO_{4d} - PO_{4h}$). The calculations in **c** and **d** are done at present-ocean conditions, i.e.,P_h = 2.31 x 10^6mol C s^{-1}, r = 169, T = 19 x $10^6 m^3$ s^{-1}, DO_h = 325 μM, and PO_{4d} = 2.15 μM(Sarmiento et al., 1988). POL, present oceanic level of dissolved oxygen. POL of high-latitude surface seawater is 325 μM(Sarmiento et al., 1988).

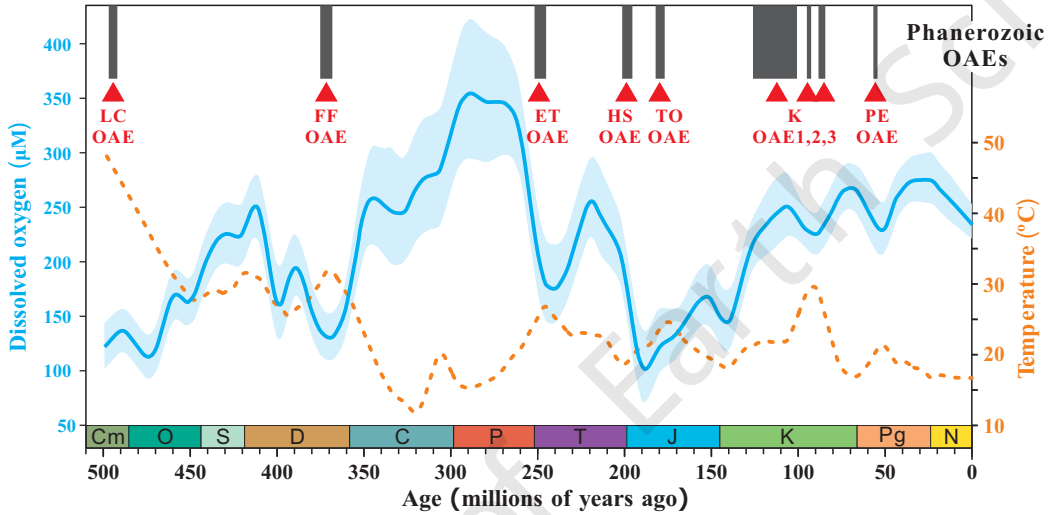

Figure 5.Dissolved oxygen, sea surfacetemperature and oceanic anoxic events for the past 500 million years. Dissolved oxygen values are calculated from temperature, atmospheric oxygen, and salinity. The temperature curve is from Figure 2. The shade shows 90% confidence interval. Oceanic anoxic events (OAEs) are compiled based on Table S2. LC, late Cambrian; FF, Frasnian-Famennian; ET, Early Triassic; HS, Hettangian-Sinemurian; TO, Toarcian; K, Cretaceous; PE, Paleocene-Eocene.

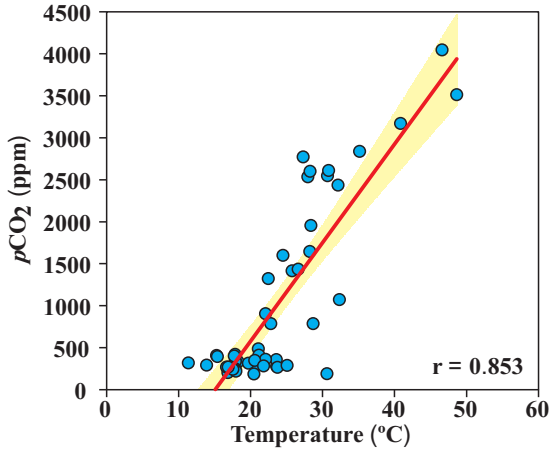

Figure 6.Cross plots of sea surfacetemperature and atmospheric carbon dioxide(r = 0.853, N = 51, *p*< 0.001; Table S3).The shade shows 95% confidence interval. Atmospheric CO_2 concentrations are from the GEOCARBSULF model(Royer et al., 2014).

Table S1. Mean sea surface temperature per million years in the Phanerozoic. Data are are from Dataset S1. *Range*$_{95\%CI}$ is the range of 95% confidence interval.

Age (Ma)	Mean temperature(°C)	Number	Range$_{95\%CI}$
0	18.22	1618	0.20
1	15.38	1053	0.11
2	16.19	1018	0.10
3	17.16	1634	0.09
4	17.47	2072	0.08
5	17.13	1506	0.09
6	15.19	222	0.26
7	15.67	60	0.55
8	16.11	51	0.89
9	16.99	72	0.66
10	18.94	74	0.82
11	17.78	90	0.58
12	16.57	68	0.84
13	15.25	152	0.20
14	16.74	35	0.81
15	17.09	30	0.96
16	17.64	21	1.13
17	16.83	27	1.12
18	15.43	38	0.93
20	16.64	36	0.82
22	19.03	45	0.93